Talanta 89 (2012) 462–469

Contents lists available at SciVerse ScienceDirect

Talanta

journal homepage: www.elsevier.com/locate/talanta

XRF, μ-XRD and μ-spectroscopic techniques for revealing the composition and structure of paint layers on polychrome sculptures after multiple restorations

M.L. Franquelo [a], A. Duran [b,*], J. Castaing [c], D. Arquillo [d], J.L. Perez-Rodriguez [a]

[a] Materials Science Institute of Seville (CSIC-University of Seville), Americo Vespucio 49, 41092 Seville, Spain
[b] Department of Chemistry and Soil Sciences, School of Sciences, University of Navarra, Irunlarrea 1, 31080 Pamplona, Spain
[c] Centre de Recherche et de Restauration des Musées de France (C2RMF-CNRS), Palais du Louvre, 14 quai François Mitterrand, 75001 Paris, France
[d] Fine Arts Faculty of Seville, University of Seville, Laraña 3, 41003 Seville, Spain

ARTICLE INFO

Article history:
Received 30 September 2011
Received in revised form
19 December 2011
Accepted 22 December 2011
Available online 28 December 2011

Keywords:
XRF portable system
Micro-XRD laboratory-made system
Micro-spectroscopy
Complex polychrome structures
Gothic sculpture

ABSTRACT

This paper presents the novel application of recently developed analytical techniques to the study of paint layers on sculptures that have been restored/repainted several times across centuries. Analyses were performed using portable XRF, μ-XRD and μ-Raman instruments. Other techniques, such as optical microscopy, SEM-EDX and μ-FTIR, were also used. Pigments and other materials including vermilion, minium, red lac, ivory black, lead white, barium white, zinc white (zincite), titanium white (rutile and anatase), lithopone, gold and brass were detected. Pigments from both ancient and modern times were found due to the different restorations/repaintings carried out. μ-Raman was very useful to characterise some pigments that were difficult to determine by μ-XRD. In some cases, pigments identification was only possible by combining results from the different analytical techniques used in this work. This work is the first article devoted to the study of sculpture cross-section samples using laboratory-made μ-XRD systems.

1. Introduction

Masterpieces are affected by time and/or the environment through the degradation of their physical integrity and aesthetic appearance. These deterioration processes start immediately after their manufacture. However, the most serious damages are frequently not produced by natural degradation processes but are due to human activity through. These changes, produced by anthropogenic action, were the result of political, religious, or social factors across time. As a result, multiple restorations/repaintings were carried out on the sculpture studied in this work, causing a complex polychromy [1].

Nowadays, it is possible to perform analysis of artworks through non-destructive techniques such as micro-Raman (μ-Raman), micro-X-ray diffraction (μ-XRD), and portable X-ray fluorescence/X-ray diffraction (XRF/XRD) [2–11]. New systems have also been developed for *in situ* analysis, some containing two different techniques in the same apparatus, such as Raman/XRF [12], Raman/FTIR [13], Raman/LIBS [14], and XRD/XRF [15–17]. One such portable XRF/XRD instrument was designed and constructed at the C2RMF (laboratory of the Centre de Recherche et de Restauration des Musées de France); it takes advantages of various devices initially designed for synchrotron radiation (SR) [16,18,19].

These portable instruments are carried to the sites of storage for artworks too heavy or too valuable to be displaced. They give access to precise information on the composition of these cultural heritage artefacts, mainly on their exteriors (a few microns deep). However, even in the case when holes in the upper layer give access to ancient layers underneath, the sensitivity and lateral resolution are frequently not good enough to ascertain the polychrome structure throughout. In addition, portable systems have difficulties analysing all parts of pieces due to the localisation, fold, geometry, and heterogeneity of the surface, among other factors. In this case, it is necessary to complement *in situ* non-destructive methods with the preparation and study of cross-section samples. In this way, the identification of the paint layers, from the support to the varnish, is possible using laboratory techniques including micro-Fourier Transform Infrared (μ-FTIR), μ-Raman, and scanning electron microscopy (SEM-EDX).

μ-XRD is used to determine crystalline phases. The development of μ-XRD has allowed the determination of crystalline pigments in very small areas not only on surfaces but also on samples taken from artwork. μ-Diffraction measurements in painting cross-sections have been performed, in most cases, with synchrotron radiation (SR) [20,21] and very rarely with other laboratory equipment [19,22]. The C2RMF laboratory at the Louvre Museum has recently designed and constructed a μ-XRD

* Corresponding author.
E-mail address: adrianduran@unav.es (A. Duran).

0039-9140/$ – see front matter © 2011 Elsevier B.V. All rights reserved.
doi:10.1016/j.talanta.2011.12.063

apparatus that takes advantage of various devices already developed for SR. Because SR facilities are not easily accessible, new μ-XRD laboratory systems are being developed to obtain similar results to SR techniques although better resolution is achieved with SR [18]. μ-Raman spectroscopy has attracted the attention of scientists working in the field of art restoration and conservation. There are several advantages of this technique, including its ability to record spectra of inorganic and organic compounds, the broad range of objects than can be investigated, the high spatial resolution (analysis of micro-samples) and the possibility to perform *in situ* investigations [23–28].

The aim of this work was thus to apply recently developed analytical techniques to the full characterisation of complex polychrome structures on a sculpture from the 13th to 14th centuries that had been restored/repainted several times. These repeated treatments formed a large number of layers of different chemical and mineralogical compositions. The portable XRF system was first used to determine the elemental composition of the upper layers before taking a few samples. Complete collection of information through the application of a dedicated laboratory-made μ-XRD combined with μ-Raman, μ-FTIR and SEM-EDX was demonstrated in the analysis of all the layers of the different cross-section samples prepared from different parts of the polychrome sculpture. Therefore, we provide a new analytical methodology for the characterisation of complex polychrome structures, combining different non-invasive and micro-invasive techniques. The complementarities of the techniques employed and the differential information they deliver are thoroughly discussed in the text.

2. Materials and methods

2.1. Materials

The triplex sculpture of polychrome wood "Our Lady Santa Ana" studied in this work represented medieval aesthetics of French origin and depicts Saint Anne, the Virgin and the Child (supplementary Fig. S1) [1]. It is dated to between the 13th and 14th centuries. This sculpture was selected because it had suffered several restorations in the course of its history, generating a complex polychromy with pigments used in both ancient and modern times. In spite of the multiple restorations, the sculpture is now in a relatively bad state. Twenty representative samples from different zones were taken from the sculpture. Samples sizes were approximately 1 mm × 1 mm and removed with a scalpel.

2.2. Methods

The cross-sections were prepared following the methodology described by Duran et al. [29,30] and Khandekar [31]. They were observed and photographed with an optical microscope (Nikon OPTIPHOT, 25×, 50× and 100×). Fig. 1 shows a selection of the cross-sections prepared from the extracted samples.

The portable XRD/XRF system had an X-ray tube (40 kV, 700 μA) with a copper anode [16]. It provided, through a 0.1 mm beryllium window, polychromatic X-rays necessary for XRF measurements. The measured area was approximately 4 mm × 3 mm with a slit of 0.5 mm at the exit of the tube. The XRF detector was a silicon drift detector (SDD) with energy resolution (full width at half-maximum) of 150 eV at 5.9 keV. It was Peltier cooled to −10 °C and located 90° to the X-ray tube and on the axis normal to the analysed sample surface (so it was placed in front of the point where X-rays impinge the surface of the object). Two laser pointers intersected at the analysis position where the X-ray beam impinged the surface of the object. The components of the apparatus are fixed on a support that can be moved along the object to be analysed. Helium flux was not used with this apparatus, thus light elements up to silicon were not detected due to the strong absorption in air between specimen and detector (≈2 cm). The time of acquisition was 300 s, and the XRF spectra were analysed using ArtTAX and PMCA software packages. Only XRF experiments were carried out because XRD was not possible due to geometrical restrictions in the sculpture shape.

μ-XRD experiments were performed on the cross-sections in reflection mode with the dedicated laboratory-made μ-XRD equipment developed at C2RMF [18]. The sample was centred using a remotely controlled head that allowed movements in the *x*, *y* and *z* directions in steps as small as 1 μm. The instrument was equipped with an optical video recording microscope and two laser alignment devices to allow accurate alignment and recording of the area from which the diffraction patterns were recorded. The Rigaku microfocus X-ray tube had a power of approximately 30 W. Collimators of 100 and 200 μm were used in this study. Imaging plates served as bi-dimensional detectors, and the collection time for each diagram was 10 min. The μ-XRD equipment uses X-ray optics to concentrate photon flux in small areas.

A dispersive integrated Horiba Jobin-Yvon LabRam HR800 μ-Raman system was employed for recording spectra. The experiments were performed directly on the cross-sections. Two external visible diode lasers (solid-state source) were available in this apparatus: 532 nm (green) and 784.5 nm (red), but we mainly used the 784.5 nm laser to minimise fluorescence of the organic medium or of the pigments themselves. The equipment had a charge-coupled device (CCD) detector and a grating of 680 grooves/nm. An optical microscope was coupled confocally to the Raman spectrometer. Almost all the measurements shown in this paper were collected at 50× and 100× magnifications (spot size approximately 5 μm × 5 μm). Each Raman spectrum was recorded for 8–12 min with a spectral resolution of 2 cm^{-1}. Power values measured during the experimental process were between 16 and 40 mW to avoid damage to the cross-sections.

μ-FTIR spectra were recorded using a Nicolet 510 apparatus (source: Globar, detector: DTGS) in reflection mode with a Nic-Plan optical microscope coupled confocally to the spectrometer. Similarly to μ-Raman, the experiments were performed directly on the cross-sections. The spot size was approximately 15 μm × 15 μm, and at least 200 scans were accumulated for each spectrum at a 4 cm^{-1} resolution.

Elemental chemical analyses over the cross-sections were obtained using a Jeol JSM 5400 SEM instrument equipped with a Link ISIS energy dispersive X-ray (EDX) analyser at an accelerating voltage of 20 kV. Samples were coated with gold or carbon film prior to analysis.

3. Results

3.1. Portable XRF study of the external layers of the polychromy

Small fragments/flakes from the exterior of the polychrome were lost in some parts of the sculpture, exposing internal zones, mainly in the face of Saint Anne (supplementary Fig. S2). In addition to the upper layer (three points: white colour (E1W and E2W) and carnation (E2C)), XRF spectra were collected in four of these internal areas (corresponding to carnation (I2C, I3C, and I4C), and black colour (I1B)). The spectra obtained in the internal (Fig. 2a) and external (Fig. 2b) layers showed some differences. Lead was present in a high proportion in all of the areas studied, except in the carnation of the exterior (E2C). Zinc was detected in all measurements carried out on the carnation and black. This element was not present in the white colour of the external areas (E1W and E2W). In one experiment carried out in a carnation zone of the internal zone (I4C), a small intensity peak attributed to mercury appeared,

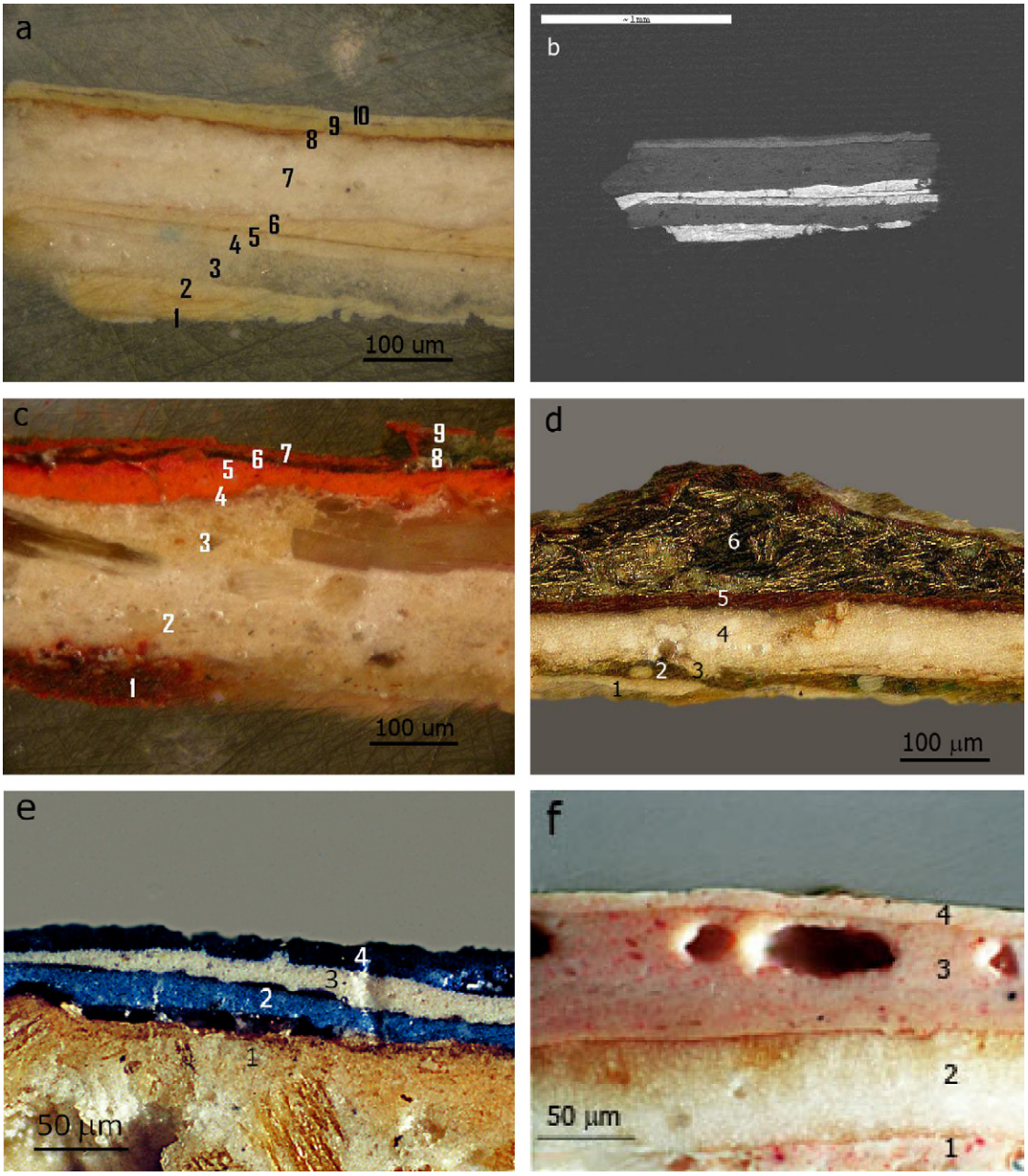

Fig. 1. Micrographs of cross-sections from samples: SA-13 (a), SA-5 (c), SA-18 (d), SA-23 (e) and SA-22 (f). SEM micrograph with backscattering for sample SA-13 (b). (For interpretation of the references to colour in the text, the reader is referred to the web version of the article.)

possibly from the presence of vermilion (HgS) (Fig. 2a). Barium and titanium were also detected in almost all the zones measured, and notable levels of barium were especially present in the carnation of the external part (E2C) and in black colour (I1B) (Fig. 2).

The analyses revealed the presence of a pigment made with zinc, possibly zinc white (zincite, ZnO). Barium and titanium detected by XRF could be assigned to the presence of barium white (barite, $BaSO_4$) and titanium white (titanium oxides, TiO_2). In the black (I1B) of the sculpture, high amounts of iron were detected by XRF analyses that might have been responsible for the brown colour of this zone (iron oxides and/or iron oxyhydroxides are suspected).

3.2. Study of the cross-sections

The portable XRF equipment provided important information on the external layers of the polychromy. However, to obtain information on the composition of all the layers in the polychrome structure, it was necessary to study cross-sections that contained all the layers. Five cross-sections, representative of the main colours observed in the sculpture, were selected for this purpose (Fig. 1). The observations by optical microscopy and SEM-EDX showed a complex composition with a high number of layers (from 4 to 10).

3.2.1. μ-XRD

Valuable information was provided by μ-XRD. The sample SA-13 was taken from the headdress of Saint Anne (supplementary Fig. S1), and the cross-section photomicrographs (Fig. 1a) showed that it contained ten layers. The images from the SEM (Fig. 1b) with backscattering electrons showed two bright zones (layers 1 and 2; and 4, 5, and 6) due to the high atomic number of the elements present in both layers. The μ-XRD study of the lower layers (approximately 1, 2 and 3) showed the presence of lead white

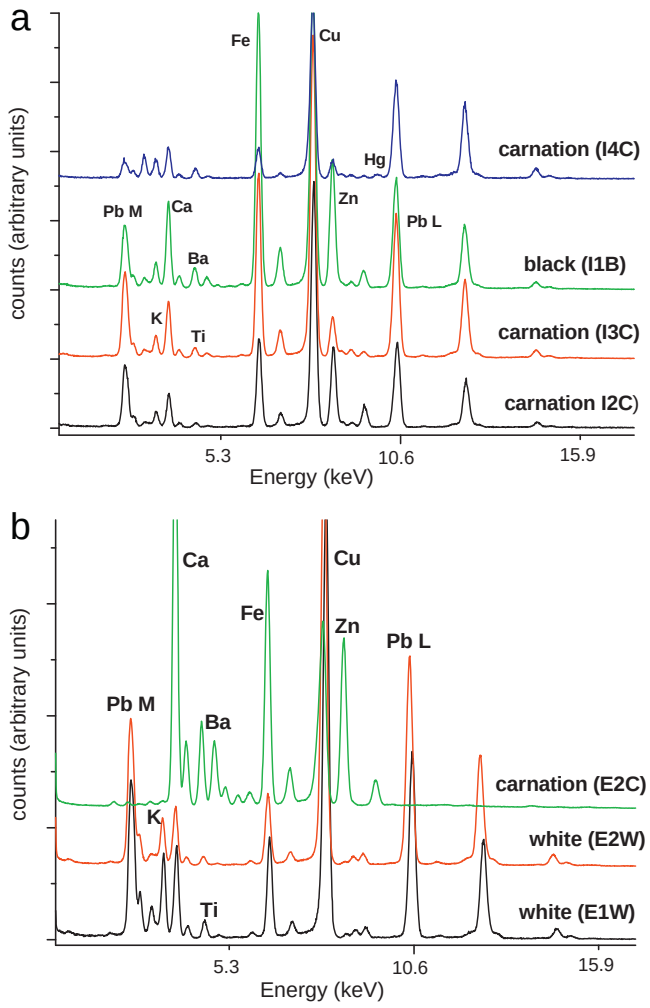

Fig. 2. XRF spectra collected on the internal areas (a) and external areas (b) of the sculpture. (For interpretation of the references to colour in the text, the reader is referred to the web version of the article.)

(hydrocerussite ($Pb_3(CO_3)_2(OH)_2$) and cerussite ($PbCO_3$)) and gypsum ($CaSO_4{\cdot}2H_2O$) (Fig. 3a). The lead white corresponded to the lowest layers (1 and 2) composed of elements of high atomic number (Fig. 1b), while only gypsum was present in layer 3. The μ-XRD

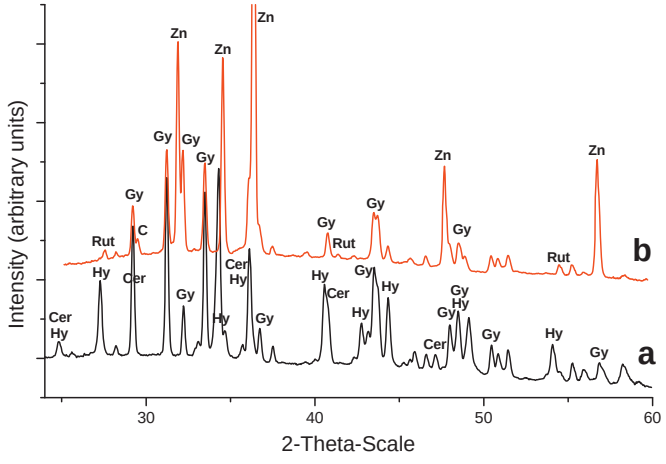

Fig. 3. μ-XRD diagrams collected on the cross-section SA-13: layers 1, 2 and 3 (a) and layers 7, 8, 9 and 10 (b). Cer = cerussite, Hy = hydrocerussite, Rut = rutile, Gy = gypsum, Zn = zincite and C = calcite.

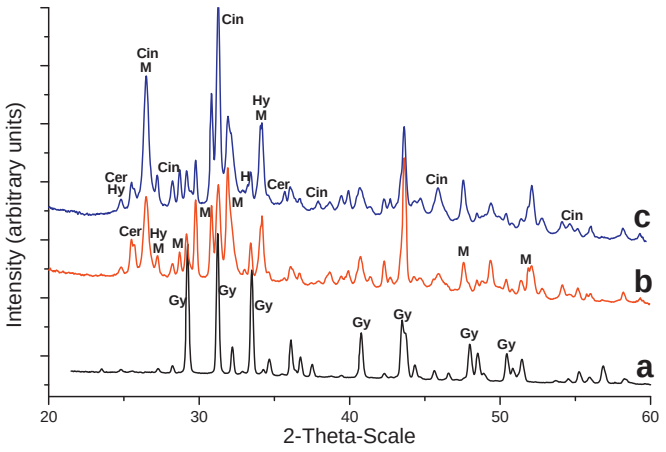

Fig. 4. μ-XRD diagrams collected on the cross-section SA-5: layers 2 and 3 (a), layers 4 and 5 (inner zone) (b), and layers 4 and 5 (upper zone) (c). Cer = cerussite, Hy = hydrocerussite, Cin = cinnabar, M = minium, H = hematite and Gy = gypsum. (For interpretation of the references to colour in the text, the reader is referred to the web version of the article.)

diagrams of approximately the layers 4, 5 and 6 showed similar compositions to the previous ones (lead white) with a very thin layer (5) situated between layers 4 and 6. The μ-XRD study of the upper layers (7, 8, 9 and 10) (Fig. 3b) showed the presence of zincite (zinc white, ZnO). In addition, small amounts of rutile (a crystalline form of titanium white, TiO_2) and calcite ($CaCO_3$) were also detected. Gypsum was also observed in layer 7.

Sample SA-5 was collected from the red dress of Saint Anne (left side of the sculpture, supplementary Fig. S1). Nine layers were observed in the cross-section (Fig. 1c). The μ-XRD study of the white layers (2 and 3) showed the presence of gypsum (Fig. 4a). The characterisation of all red layers located at the top of the cross-section was difficult because five coloured layers were observed by optical microscopy and SEM-EDX in a narrow zone. However, the XRD diagram of the approximately lower red layers (4 and 5, Fig. 4b) showed the presence of cinnabar (vermilion pigment, HgS) and minium (Pb_3O_4), both being red pigments. In addition, cerussite, hydrocerussite and gypsum were detected. The gypsum was probably released from the lower layer (3). The diagram obtained from the upper red zone (also in layers 4 and 5, but several microns higher) showed similar composition to the other inner red zone (Fig. 4c). However, the intensities of the minium peaks decreased, as did the cerussite and hydrocerussite peaks, while the intensities of the cinnabar peaks increased. These results suggested the presence of two layers, one lower mainly composed of minium, cerussite and hydrocerussite, and one upper mainly formed from cinnabar, cerussite and hydrocerussite. In the latter μ-XRD diagram (Fig. 4c), a peak of small intensity also appeared at $d = 0.269$ nm ($2\theta = 33^\circ$), suggesting the presence of hematite (iron oxide, Fe_2O_3).

The gilding was studied in sample SA-18 (Fig. 1d), and gypsum and brass were detected by μ-XRD. Main diffraction peaks of brass (Cu–Zn alloy) were observed at $d = 0.212$ nm ($2\theta = 42.5^\circ$) and $d = 0.183$ nm ($2\theta = 49.7^\circ$).

Sample SA-23 was taken from the blue dress of St Anne (supplementary Fig. S1). The cross-section (Fig. 1e) showed the following layers: a broad layer of white at the bottom (1) followed by three layers of blue (2), white (3) and blue (4), respectively. The μ-XRD study of the broad white layer (1) showed the presence of gypsum (Fig. 5a). The μ-XRD diffractions of the inner blue layer (2) showed zincite as the major component, with gypsum (coming from the lower layer), calcite and lazurite [$Na_8(Al_{12-x}Si_xO_{24})S_n$] in lower proportions, the latter responsible for the blue colour (Fig. 5b). The white layer (3), observed between the two blue layers,

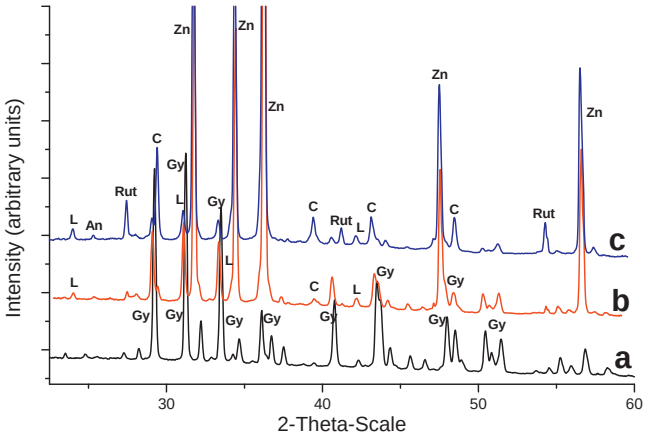

Fig. 5. μ-XRD diagrams collected on the cross-section SA-23: layer 1 (a), layer 2 (b), and layer 3 and 4 (c). L = lazurite, An = anatase, Rut = rutile, C = calcite, Zn = zincite and Gy = gypsum. (For interpretation of the references to colour in the text, the reader is referred to the web version of the article.)

was mainly composed of zincite. In addition, rutile, anatase (titanium white, TiO_2) and calcite were also found by μ-XRD. The upper layer of blue colour (4) was composed of zincite, calcite, anatase, rutile and lazurite (Fig. 5c). According to the continuous rings seen for the lazurite diffractions in the 2D XRD detector, we suspected the presence of artificial lazurite.

Sample SA-22 was taken from the neck of the Virgin (supplementary Fig. S1). The cross-section (Fig. 1f) showed two layers of carnation (1 and 3) separated by another layer of white (2). The μ-XRD showed the presence of gypsum in the white layer, whereas the layers of carnation contained hydrocerussite, cerussite and a small amount of cinnabar (vermilion), responsible for the reddish colour.

3.2.2. μ-Raman

μ-Raman was used to study the pigments in the red layers that were not detected by μ-XRD (see Section 3.2.1). The Raman spectra of the small layer of dark red colour (1) that appeared at the bottom of sample SA-5 (Fig. 1c) showed the presence of hematite and silicates (Fig. 6a). The bands at 251, 280 and 343 cm^{-1} and the bands

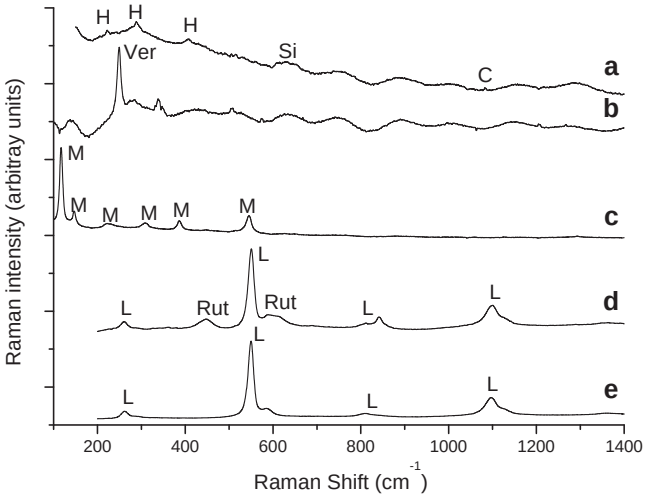

Fig. 6. μ-Raman spectra of the different layer samples: dark red (1) of SA-5 (a), red (4) of SA-5 (b), red (5) of SA-5 (c), inner blue (2) of SA-23 (d), and superficial blue (4) of SA-23 (e). H = hematite, Si = silicate, Ver (Cin) = vermilion, M = minium, L = lazurite, Rut = rutile, C = calcite. (For interpretation of the references to colour in this figure legend, the reader is referred to the web version of the article.)

at 118, 147, 221, 307, 386 and 546 cm^{-1} were attributed to vermilion (Fig. 6b) and minium (Fig. 6c), respectively, detected in layers 4 and 5. Raman spectroscopy also detected the presence of iron oxides and silicates in layers 8 and 9, corresponding to the upper red zone. These data confirmed that the peak at $2\theta = 33^{\circ}$ observed by μ-XRD and the iron detected by SEM-EDX belonged to iron oxide pigments from the most external layers.

The Raman spectrum (Fig. 6d) of the inner blue layer of sample SA-23 (Fig. 1e) showed the presence of lazurite (bands at 260, 549, 1098 and 1102 cm^{-1}), in agreement with the μ-XRD results. Furthermore, the bands at 447 and 609 cm^{-1} were attributed to rutile. The Raman spectrum (Fig. 6e) of the superficial blue layer (4) of the same sample showed bands at 260, 549, 1098 and 1102 cm^{-1}, attributed to lazurite. Due to its application in a recent restoration carried out in 1966 to eliminate an insect attack, combined with the μ-XRD data (see Section 3.2.1), the presence of artificial lazurite (ultramarine blue) was suggested.

The Raman spectrum of the thin layer (4) of sample SA-22 (Fig. 1f) showed the presence of zincite, rutile and calcite. Zinc white is a particularly difficult pigment to detect by Raman spectroscopy as it is highly fluorescent, but in our case, it was detected thanks to its Raman bands at 433 and 377 cm^{-1}. These minerals were also found in layers 9 and 10 of sample SA-13 (Fig. 1a). These results matched those derived from the μ-XRD data.

3.2.3. SEM-EDX and μ-FTIR

The EDX analysis of a black sample collected from a black colour zone (I1B) showed the presence of phosphorus and calcium (Fig. 7a), suggesting that the black colour was given by ivory black (mainly calcium phosphate, $Ca_3(PO_4)_2$ + carbon, C). XRF analyses agreed with those from EDX. Although unfortunately phosphorus was not detected (Fig. 2a) due to the experimental constraints of the XRD/XRF apparatus, calcium peak is clearly observed.

Iron, silicon, aluminium and potassium were detected by EDX (Fig. 7b) in the small layer of dark red colour at the bottom of the cross-section of sample SA-5 (Fig. 1c), in agreement with the μ-Raman results (see Section 3.2.2). The characterisation of all red layers located at the top of the cross-section was more difficult because five coloured layers with different elemental compositions were confirmed by SEM-EDX analyses in a narrow zone. EDX analysis showed two layers (4 and 5), one layer containing mercury, sulphur and lead and another layer with only lead. This observation confirmed the presence of cinnabar mixed with lead white and another layer of minium and lead white determined by μ-XRD and μ-Raman spectroscopy. In the red zone, the EDX analysis showed another layer (6) containing aluminium with lead, calcium and carbon (Fig. 7c), which suggested the presence of a red lac impossible to characterise by XRD due to its amorphous character.

μ-FTIR spectra of layer 6 showed absorption bands at 1643 and 1406 cm^{-1} of υ(C=O) and 1138 cm^{-1}, attributed to the presence of the calcium salt of carminic acid. These data agreed with the presence of red lac suggested by EDX [32]. Layer 7 was composed of a resin, as confirmed by μ-FTIR spectra bands (2869, 2946 cm^{-1} assigned to the C—H elongation vibrations, 1695 cm^{-1} to C=O and 1643 cm^{-1} to C—C) [33]. Layers 8 and 9 were small, narrow and not continuous, so they could not be studied by μ-XRD. The EDX analysis of these two upper layers detected sulphur, calcium, barium, iron, zinc, silicon and aluminium (Fig. 7d). The presence of sulphur, barium and zinc suggested the presence of lithopone ($BaSO_4$ + ZnS), barium white and/or zincite. The iron might have been responsible for the red colour (Fig. 1c) that appeared in these most external layers.

The brown colour that appeared in layer 8 of the cross section of sample SA-13 (Fig. 1a) was produced by a resin, similarly to layer 5, as confirmed by μ-FTIR (bands at 2869, 2944 cm^{-1} assigned to

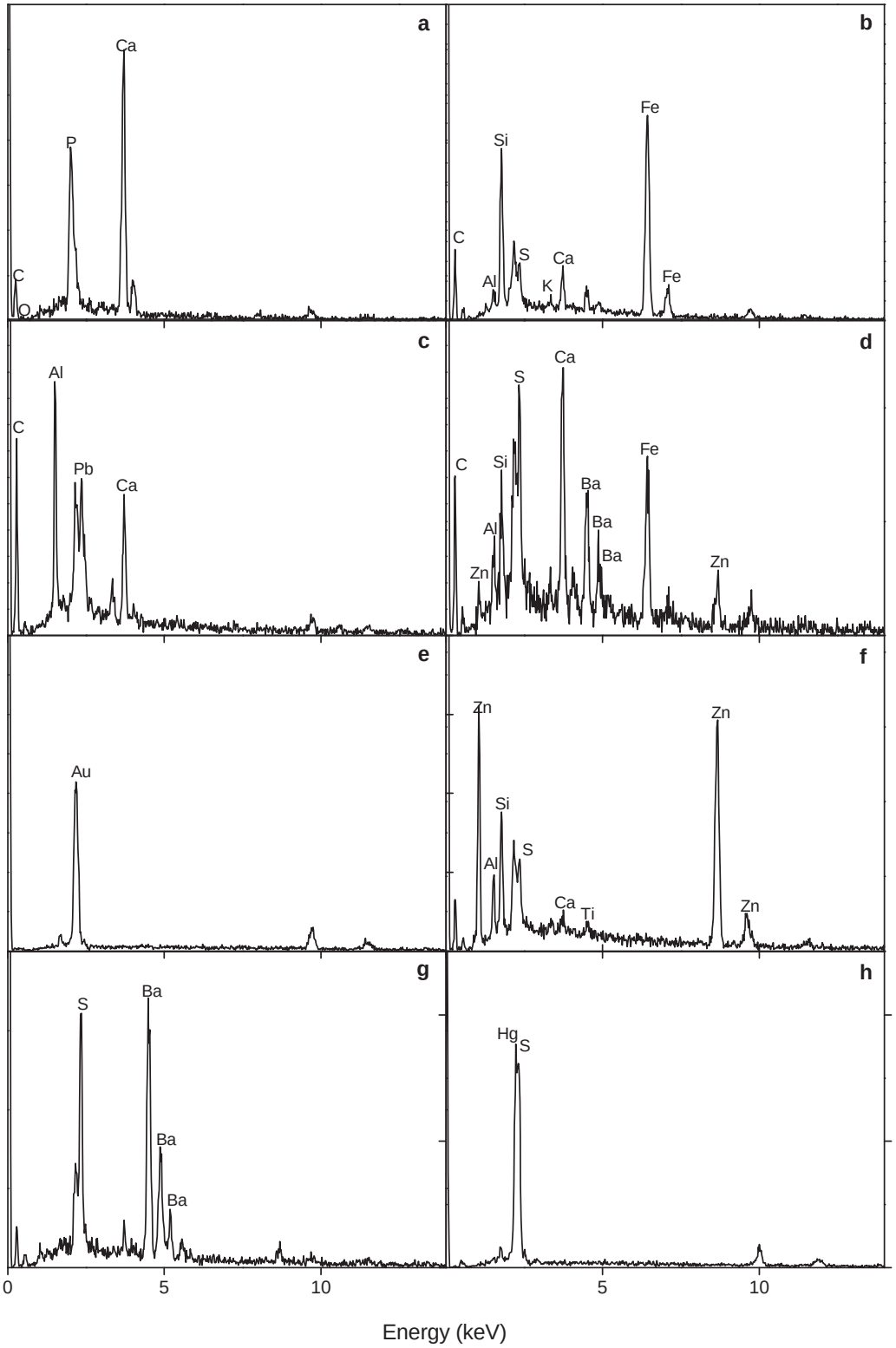

Fig. 7. SEM-EDX analysis carried out on the different studied samples: black fragment in zone I1C (a), dark red layer (1) of sample SA-5 (b), red layer (6) of SA-5 (c), red layers 8–9 of SA-5 (d), top of layer (6) or layer (7) of SA-18 (e), white layer (3) of SA-23 (f and g), and carnation layer (3) of SA-22 (h). (For interpretation of the references to colour in this figure legend, the reader is referred to the web version of the article.)

C—H elongation vibrations, 1696 cm^{-1} to C=O and 1641 cm^{-1} to C—C) [33].

The gilding was observed in sample SA-18 (Fig. 1d). At the bottom, a layer of lead-based compounds (1) appeared, followed by another layer of copper (2) covered with another of lead-based compounds (3). Layer 4 contained compounds based on calcium and sulphur, possibly gypsum, followed by a burnish layer (5) composed of iron, aluminium, silicon (possibly clay minerals) and lead compounds. The gilding (6) was made with brass (copper and zinc), as mentioned before thanks to μ-XRD analyses (see Section 3.2.1).

Finally at the top of the polychrome (6), gold appeared (Fig. 7e). This gilding was first made with false gold then covered with gold leaf during a later restoration that had practically disappeared (7).

The EDX analyses of the white layer (3) of sample SA-23 (Fig. 1e) observed between the two blue layers showed the presence of zinc, barium, titanium and sulphur (Fig. 7f and g). Using μ-XRD, the presence of rutile, anatase and calcite was found in this same layer. EDX analyses confirmed the presence of vermilion due to the detection of sulphur and mercury (Fig. 7h) in layers 1 and 3 of sample SA-22 (Fig. 1f).

4. Discussion

For XRF, the depth of analysis depends on the nature of the elements assayed and also on the energy of the fluorescing X-rays used for the detection of the elements (e.g., Pb–L $E = 9.2–15.8$ keV or Pb–M $E = 2.3–2.6$ keV). For instance, the theoretical penetration in a layer composed of pure cerussite is approximately 1.5–2 μm at $E = 8.0$ keV (Cu–Kα radiation) and at X-rays beam incidence angle of 10° [34]. The presence of lead in almost all the external areas of the sculpture and the thickness of the polychromy (200–500 μm approximately, Fig. 1) limited the amount of information obtained by XRF to only the exterior of the polychrome. Access to lower layers through occasional holes was not sufficient to determine the entire complex structure of the polychromy.

Iron is almost always present in XRF spectra because Fe fluorescence is strongly excited by the copper radiation used as the X-ray source [16]. Iron oxides and/or iron oxyhydroxides are suspected if the iron amount is very high; in other cases, iron could be assigned to the presence of rests and/or contamination (iron-compounds in very low concentration). However, light elements are not detected by this technique because of the strong absorption in the beryllium window (from detector) and in air (2–3 cm) between the sample and the XRF detector. X-ray transmission in air is only about 5% for a 3 cm path and 40% for a 1 cm path at Si–K energy (1.7 keV) [16,35]. The detection limits for light elements could be improved by reducing the distance between the sample and the detector or by replacing the air with helium [35,36]. In our case, phosphorus detected by EDX could not be detected by XRF due to the limitations mentioned above. XRD is therefore essential to identify compounds materials that often contain light elements (e.g., oxides, carbonates, and phosphates).

To obtain information on the composition of all the layers of polychromes structure, it was necessary to study representative cross-sections that contained all the layers of interest. Although the analysed areas were approximately 0.01 and 0.04 mm^2 for μ-XRD experiments when using collimators of 100 and 200 μm, respectively, and the different measurements did not correspond exactly to each layer in the cross-section, we were still able to obtain data on the different layers without much effort with a proper interpretation of the collected results as shown in this study. Furthermore, the technique developed here was micro-invasive because only minor amounts of sample are necessary for measurements, in contrast to conventional X-ray powder diffraction. In this case, the bad state of the artwork made the removal of small samples acceptable. Finally, the samples can be used for other analyses or archived following μ-XRD.

μ-XRD was not a completely adequate technique for the characterisation of the two red pigments in layers 4 and 5 of sample SA-5 (Fig. 1c) due to the size of the X-ray beam. μ-Raman was therefore used for the accurate characterisation of these two layers of red colour. The zone analysed by Raman was approximately 5 μm × 5 μm, a size that allowed differential analyses of each red colour in these thin layers. This was just one illustration of μ-Raman as a good technique for characterising the composition of very narrow samples.

Imaging and elemental microanalysis of cross-sections by SEM-EDX was a valuable tool in this study, particularly for the complex polychrome structure. SEM-EDX microanalysis provided information on elements with atomic numbers larger than 6. It should be noted that this technique cannot differentiate between samples with similar elemental composition but different stoichiometry, especially when they contain light elements (e.g., carbon, oxygen and nitrogen).

The presence of organic matter cannot be directly established by XRD, XRF or SEM-EDX. However, μ-FTIR has been a useful technique to determine the presence of resin and red lac pigment. In this work, this technique was also used for the characterisation of compounds containing inorganic polyatomic anions.

The results obtained for the external layers of cross-sections of carnation colour in sample SA-22 (Fig. 1f) and for the white colour of sample SA-13 (Fig. 1a) matched those derived from XRF in exterior studies (Fig. 2). Mercury, zinc, barium and titanium identified by the portable system are according to the detection of compounds as cinnabar, zincite and rutile detected by other techniques applied on the upper layers of the cross-sections.

The compositions of all the layers in the cross-sections were successfully determined. The techniques used for this characterisation were based on elemental analysis (XRF and SEM-EDX) and μ-XRD. These two sets of techniques provide quality information for the characterisation of different inorganic pigments present in the layers of a polychrome on a cultural heritage object. However, pigment identification was not possible in some cases because of the poor spatial resolution of μ-XRD. In our case, we had to combine results from other analytical techniques to circumvent this issue.

Due to these analytical results, the story of restoration through the centuries could be related to the curators/conservators in charge of the artwork. For example, the pigment zincite appeared commercially in the 19th century and is a non-poisonous but mildly antiseptic compound. It requires more oil to form a paste than lead white (mixtures of cerussite and hydrocerussite) and has a tendency to eventually dry out and become brittle and crack. Barium white and titanium white (titanium oxides) are pigments that were used in connection with paints since the end of the 19th or beginning of the 20th century [37]. Ultramarine blue (artificial lazurite) was first used in paintings around 1830, and lithopone has only been used recently, suggesting these pigments were used in recent restorations. Vermilion, minium, lead white, hematite, red lac, gold, brass, calcite and gypsum are all pigments that have been used since ancient times.

5. Conclusions

The sculpture studied in this work had been restored/repainted several times across centuries, which was responsible for the complex polychrome with many layers (preparation, paints and repaints) on the piece detected by optical and scanning electron microscopes. The layers showed different chemical and mineralogical compositions, which made their complete characterisation difficult.

XRF provided a quick and easy view of the compounds present on the exterior of the polychromy. μ-XRD proved to be a highly effective method for non-destructive analysis of the different layers of the polychrome cross-sections. The main limitation of μ-XRD was the spatial resolution, which made the characterisation of the thin layers of the polychromy difficult. This difficulty could be overcome using μ-Raman. Alternatively, SEM-EDX microanalysis on cross-sections also provided valuable information on the chemical elements present in each layer. Notably, the results derived from

these different techniques were all in agreement. In some cases, the complementary use of different techniques was necessary for the full identification of the compounds present in the polychromy.

This is the first article devoted to the study of the cross-sections of a polychrome sculpture using a laboratory-made μ-XRD system.

The analyses carried out by these techniques identified vermilion, minium, lead white, hematite, red lac, gold, brass and gypsum in the artwork, all utilized since antiquity. Titanium white (rutile, anatase), barium white, zinc white, lithopone, lazurite and gold were also identified in this study and were applied more recently.

Acknowledgements

The authors acknowledge assistance from C2RMF, the Fine Arts Faculty of Seville staff, as well as the program EU-ARTECH (FP6, European Union, contract RII3-CT-2004-506171).

Appendix A. Supplementary data

Supplementary data associated with this article can be found, in the online version, at doi:10.1016/j.talanta.2011.12.063.

References

[1] F. Arquillo, Dictamen histórico, artístico, científico y técnico de la imagen triplex representando a Santa Ana, la Virgen y el Niño, Facultad de Bellas Artes Universidad de Sevilla, Sevilla, 2010.
[2] S. Bruni, S. Caglio, V. Guglielmi, G. Poldi, Appl. Phys. A 92 (1) (2008) 103–108.
[3] K. Castro, N. Proietti, E. Princi, S. Pessanha, M.L. Carvalho, S. Vicini, D. Capitani, J.M. Madariaga, Anal. Chim. Acta 623 (2) (2008) 187–194.
[4] R.J.H. Clark, J. van der Weerd, J. Raman Spectrosc. 35 (4) (2004) 279–283.
[5] A. Duran, M.L. Franquelo, M.A. Centeno, T. Espejo, J.L. Perez-Rodriguez, J. Raman Spectrosc. 42 (1) (2011) 48–55.
[6] A. Duran, J.L. Perez-Rodriguez, T. Espejo, M.L. Franquelo, J. Castaing, P. Walter, Anal. Bioanal. Chem. 395 (7) (2009) 1997–2004.
[7] A. Duran, M.B. Siguenza, M.L. Franquelo, M.C.J. de Haro, A. Justo, J.L. Perez-Rodriguez, Anal. Chim. Acta 671 (1–2) (2010) 1–8.
[8] W. Faubel, S. Staub, R. Simon, S. Heissler, A. Pataki, G. Banik, Spectrochim. Acta B 62 (6–7) (2007) 669–676.
[9] A. Jurado-Lopez, O. Demko, R.J.H. Clark, D. Jacobs, J. Raman Spectrosc. 35 (2) (2004) 119–124.
[10] S. Svarcova, E. Koci, P. Bezdicka, D. Hradil, J. Hradilova, Anal. Bioanal. Chem. 398 (2) (2010) 1061–1076.
[11] G. van Der Snickt, W. de Nolf, B. Vekemans, K. Janssens, Appl. Phys. A 92 (1) (2008) 59–68.
[12] K.S. Andrikopoulos, S. Daniilia, B. Roussel, K. Janssens, J. Raman Spectrosc. 37 (10) (2006) 1026–1034.
[13] F. Adar, G. LeBourdon, J. Reffner, A. Whitley, Spectroscopy 18 (2) (2003) 34–40.
[14] A. Giakoumaki, I. Osticioli, D. Anglos, Appl. Phys. A 83 (4) (2006) 537–541.
[15] G. Chiari, Nature 453 (7192) (2008) 159.
[16] A. Gianoncelli, J. Castaing, L. Ortega, E. Dooryhee, J. Salomon, P. Walter, J.L. Hodeau, P. Bordet, X-ray Spectrom. 37 (4) (2008) 418–423.
[17] P. Sarrazin, D. Blake, S. Feldman, S. Chipera, D. Vaniman, D. Bish, Powder Diffr. 20 (2) (2005) 128–133.
[18] A. Duran, J. Castaing, P. Walter, Appl. Phys. A 99 (2) (2010) 333–340.
[19] A. Duran, J.L. Perez-Rodriguez, M.C.J. de Haro, Anal. Bioanal. Chem. 394 (6) (2009) 1671–1677.
[20] L.K. Herrera, M. Cotte, M.C.J. de Haro, A. Duran, A. Justo, J.L. Perez-Rodriguez, Appl. Clay Sci. 42 (1–2) (2008) 57–62.
[21] E. Welcomme, P. Walter, P. Bleuet, J.L. Hodeau, E. Dooryhee, P. Martinetto, M. Menu, Appl. Phys. A 89 (4) (2007) 825–832.
[22] E. Bontempi, D. Benedetti, A. Massardi, A. Zacco, L. Borgese, L.E. Depero, Appl. Phys. A 92 (1) (2008) 155–159.
[23] C.L. Aibeo, S. Goffin, O. Schalm, G. van der Snickt, N. Laquiere, P. Eyskens, K. Janssens, J. Raman Spectrosc. 39 (8) (2008) 1091–1098.
[24] L. Bellot-Gurlet, S. Pages-Camagna, C. Coupry, J. Raman Spectrosc. 37 (10) (2006) 962–965.
[25] M.L. Franquelo, A. Duran, L.K. Herrera, M.C.J. de Haro, J.L. Perez-Rodriguez, J. Mol. Struct. 924–926 (2009) 404–412.
[26] I. Karapanagiotis, E. Minopoulou, L. Valianou, S. Daniilia, Y. Chryssoulakis, Anal. Chim. Acta 647 (2) (2009) 231–242.
[27] D. Lau, C. Villis, S. Furman, M. Livett, Anal. Chim. Acta 610 (1) (2008) 15–24.
[28] P. Vandenabeele, M.C. Christensen, L. Moens, J. Raman Spectrosc. 39 (8) (2008) 1030–1034.
[29] A. Duran, M.C.J. de Haro, J.L. Perez-Rodriguez, M.L. Franquelo, L.K. Herrera, A. Justo, Archaeometry 52 (2010) 286–307.
[30] A. Duran-Benito, L.K. Herrera-Quintero, M.D. Robador-Gonzalez, J.L. Perez-Rodriguez, Color Res. Appl. 32 (6) (2007) 489–495.
[31] N. Khandekar, Rev. Conserv. 4 (2003) 52–64.
[32] P.L. Lang, M.V. Orna, L.J. Richwine, T.F. Mathews, R.S. Nelson, Microchem. J. 46 (2) (1992) 234–248.
[33] A. Duran, Metodología de Estudio y Análisis de Diferentes Tipos de Obras de Arte Pertenecientes a la Escuela Sevillana de los Siglos XVII y XVIII, Universidad de Sevilla, Sevilla, 2006.
[34] B.L. Henke, E.M. Gullikson, J.C. Davis, Atom. Data Nucl. Data Tables 54 (2) (1993) 181–342.
[35] L. de Viguerie, A. Duran, A. Bouquillon, V.A. Sole, J. Castaing, P. Walter, Anal. Bioanal. Chem. 395 (7) (2009) 2219–2225.
[36] S. Pages-Camagna, E. Laval, D. Vigears, A. Duran, Appl. Phys. A 100 (3) (2010) 671–681.
[37] R.J. Gettens, G.L. Stout, Painting Materials. A Short Encyclopaedia, Dover Publications Inc., New York (EEUU), 1966.